Since January 2020 Elsevier has created a COVID-19 resource centre with free information in English and Mandarin on the novel coronavirus COVID-19. The COVID-19 resource centre is hosted on Elsevier Connect, the company's public news and information website.

Chemical Physics Letters 777 (2021) 138727

Contents lists available at ScienceDirect

Chemical Physics Letters

journal homepage: www.elsevier.com/locate/cplett

Research paper

Low rotational barriers for the most dynamically active methyl groups in the proposed antiviral drugs for treatment of SARS-CoV-2, apilimod and tetrandrine

Eugene Mamontov *, Yongqiang Cheng, Luke L. Daemen, Alexander I. Kolesnikov, Anibal J. Ramirez-Cuesta, Matthew R. Ryder, Matthew B. Stone

Neutron Scattering Division, Oak Ridge National Laboratory, Oak Ridge, TN 37831, USA

ARTICLE INFO

Keywords:
Molecular drugs
Microscopic dynamics
DFT calculations
Inelastic neutron scattering
Quasielastic neutron scattering

ABSTRACT

A recent screening study highlighted a molecular compound, apilimod, for its efficacy against the SARS-CoV-2 virus, while another compound, tetrandrine, demonstrated a remarkable synergy with the benchmark antiviral drug, remdesivir. Here, we find that because of significantly reduced potential energy barriers, which also give rise to pronounced quantum effects, the rotational dynamics of the most dynamically active methyl groups in apilimod and tetrandrine are much faster than those in remdesivir. Because dynamics of methyl groups are essential for biochemical activity, screening studies based on the computed potential energy profiles may help identify promising candidates within a given class of drugs.

1. Introduction

Even though approval and widespread use of vaccines are expected to curb the COVID-19 pandemic, the disease is not anticipated to disappear altogether but remain in circulation, albeit hopefully with reduced infection rates. This necessitates the development of medications for the treatment of COVID-19, which, in the absence of explicitly designed drugs, relies on repurposing existing antiviral drug candidates. Clinically used against COVID-19, the antiviral drug remdesivir, which was developed to treat RNA viruses [1] is converted intracellularly into metabolites that interfere with the action of the viral RNA polymerase and suppress the viral RNA production [2,3]. Even though remdesivir demonstrates antiviral activity against SARS-CoV-2 *in vitro* [4], the limited clinical efficacy has prompted a conditional recommendation against its use to treat the coronavirus disease [5] thus necessitating the search for more effective antiviral agents. An extensive screening study that analyzed *in vitro* efficacy against SARS-CoV-2 of various antivirals using remdesivir as a benchmark identified a few promising drug candidates [6]. In particular, a Ca^{2+}channel-blocking plant-derived alkaloid hanfangchin A [7] commonly known as tetrandrine from the plant name *Stephania tetrandra*, which previously demonstrated efficacy against Ebola virus [8] exhibited a remarkable level of synergy with remdesivir, significantly improving the anti-SARS-CoV-2 efficacy of this benchmark drug [6]. The efficacy of tetrandrine against SARS-CoV-2 was also discussed in different studies [9]. Moreover, an interleukin- and lipid kinase enzyme-inhibitor apilimod, which also have previously demonstrated efficacy against Ebola, Lassa, and Marburg viruses [10,11] emerged as a clear frontrunner in this screening study of the anti-SARS-CoV-2 drugs, uniquely exhibiting antiviral activity both *in vitro* and in an *ex vivo* lung culture [6]. Apilimod's high efficacy against SARS-CoV-2 was also confirmed independently [12]. However, it has also been reported that the immunosuppression observed in many COVID-19 patients might be aggravated by apilimod [13] and it is prudent to say that there are many possible candidates [14] but no universally accepted drug candidate for SARS-CoV-2.

Although the primary action mechanisms involved may be highly drug-specific, on the fundamental level, the effectiveness of the formation of the ligand-receptor complex between the target receptor and the drug (ligand) is ultimately governed by the biomolecular thermodynamics. Besides, biochemical reactions typically must be catalyzed to attain a thermodynamically favorable reaction state within a reasonable amount of time. At the macromolecular level, biocatalysis is generally performed by enzymes lowering the inter-state activation energies. At the molecular level, the small-amplitude atomic motions enable efficient exploration of the configurational states of the energy landscape [15] to sample the potentially thermodynamically favorable reaction states.

* Corresponding author.
E-mail address: mamontove@ornl.gov (E. Mamontov).

https://doi.org/10.1016/j.cplett.2021.138727
Received 27 February 2021; Received in revised form 3 May 2021; Accepted 5 May 2021
Available online 8 May 2021

Among the small-amplitude atomic motions, methyl group rotations are important because of the relative ease of thermal activation [16]. Indeed, besides the altered solubility, the improved binding affinity and metabolism are considered among the main benefactors of the increased drug potency achieved through methylation [17–19]. Using inelastic (INS) and quasielastic (QENS) neutron scattering, recognized as powerful tools for probing methyl group dynamics [20] here we demonstrate that the most dynamically active methyl groups (those with the lowest rotational barrier) experience low barriers in apilimod and tetrandrine compared to that in remdesivir. These methyl groups are associated with the pronounced quantum effects as observable at cryogenic temperatures and much faster methyl rotations at physiological temperatures for apilimod and tetrandrine compared to remdesivir. We hypothesize that there may be a link between these low barriers in apilimod and tetrandrine and their high biopharmaceutical potency that can manifest itself, in particular, in the high antiviral efficacy of these drugs, including against SARS-CoV-2, which remdesivir with its higher rotational barrier may be lacking.

2. Experimental and computational details

Apilimod and tetrandrine powders were purchased from InvivoChem LLC and used as received (their diffraction patterns are presented in Fig. 1). X'Pert Panalytical, a powder x-ray diffractometer with a Cu anode, was operated at 45 kV and 40 mA (Cu K-alpha, 1.5406 Å, 8.04 keV). Data sets were collected at room temperature. The x-ray diffraction data for apilimod could be indexed by DICVOL to a monoclinic structure (a = 14.82 Å, b = 15.22 Å, c = 19.30 Å, α = 90°, β = 98.01°, γ = 90°), with no visible impurities. The x-ray diffraction (XRD) data for tetrandrine could be indexed by TREOR to an orthorhombic structure (a = 7.06 Å, b = 12.21 Å, c = 38.40 Å), with no visible impurities. The neutron diffraction (ND) data, despite the large incoherent scattering from hydrogen atoms in the samples, can be used qualitatively to rule out certain polymorphic structures. The diffraction pattern for the only known crystal structure of apilimod (monoclinic, a = 14.94 Å, b = 15.04 Å, c = 19.42 Å, α = 90°, β = 98.13°, γ = 90° [21]) agrees well with the ND data. For tetrandrine, in which polymorphism is known, the orthorhombic crystal structure (a = 7.12 Å, b = 11.92 Å, c = 38.30 Å [22]) agrees well with the ND data, whereas the alternative crystal structures do not. Thus, the ND data can be used to distinguish among the polymorphic structures in the sample, even when the XRD data is not available. E.g., there was no XRD data measured from the remdesivir sample reported previously [23], yet the ND data from that sample agree well with the monoclinic crystal structure (a = 10.53 Å, b = 12.81 Å, c = 11.11 Å, α = 90°, β = 100.02°, γ = 90°, designated Form II [24–26]) whereas the alternative structures (designated Form I and Form III [24–26]) do not. Among the four documented polymorphs of remdesivir [24–26] Form IV was unstable and converted to Form II in solution, whereas Form III was observed in the presence of dichloromethane. Form II appears to be the thermodynamically most stable form (e.g., see [27] for a detailed review of several antivirals, including remdesivir).

As one can expect from water-insoluble compounds, apilimod and tetrandrine powders have exhibited neither weight uptake from air exposure nor weight loss from exposure to vacuum. 0.5 g of each sample was loaded and hermetically sealed with indium wire in aluminum flat-plate sample holders of 0.5 mm thickness, 30 mm width, and 50 mm height. The parameters of the BASIS [28], SEQUOIA [29], and VISON [30] neutron spectrometers used for the measurements have been described previously [23,31]. Density functional theory (DFT) calculations were performed using the Vienna Ab initio Simulation Package (VASP) [32]. The calculations used the Projector Augmented Wave (PAW) method [33,34] to describe the effects of core electrons and the Perdew-Burke-Ernzerhof (PBE) [35] exchange–correlation functional. An energy cutoff of 800 eV was used for the valence electron plane-wave basis. The total energy tolerance for electronic energy minimization was 10^{-8} eV and 10^{-7} eV for the structure optimization. The maximum

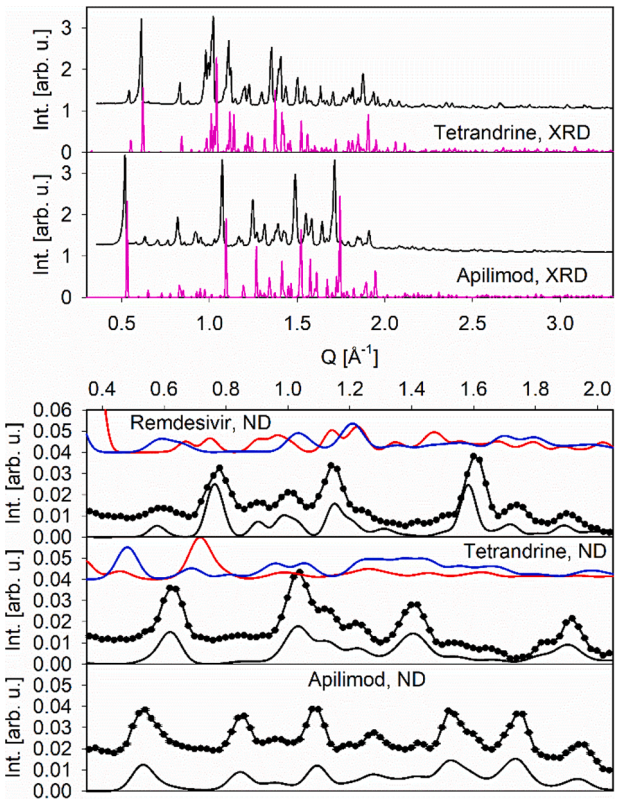

Fig. 1. Top panels: X-ray diffraction data (XRD), measured (black lines displaced vertically by one unit) and computed (pink lines) using the orthorhombic crystal structure (a = 7.12 Å, b = 11.92 Å, c = 38.30 Å [22]) for tetrandrine and the monoclinic crystal structure (a = 14.94 Å, b = 15.04 Å, c = 19.42 Å, α = 90°, β = 98.13°, γ = 90° [21]) for apilimod. Bottom panels: neutron diffraction data (ND) collected at the SEQUOIA spectrometer (symbols) and computed (solid lines). The only known crystal structure for apilimod (monoclinic, a = 14.94 Å, b = 15.04 Å, c = 19.42 Å, α = 90°, β = 98.13°, γ = 90° [21]) agrees well with the ND data. For tetrandrine, in which polymorphism is known, the orthorhombic crystal structure (a = 7.12 Å, b = 11.92 Å, c = 38.30 Å [22]), as presented by the solid black line, agrees well with the diffraction data, whereas the alternative crystal structures, as presented by the red and blue solid lines vertically displaced for clarity, do not agree with the diffraction data. For remdesivir, in which polymorphism is known, the monoclinic crystal structure (a = 10.53 Å, b = 12.81 Å, c = 11.11 Å, α = 90°, β = 100.02°, γ = 90° - Form II in [24–26]), as presented by the solid black line, agrees well with the ND data, whereas the alternative crystal structures, as presented by the red (Form I in [24–26]) and blue (Form III in [24–26]) solid lines vertically displaced for clarity, do not agree with the diffraction data.

interatomic force after relaxation was below 0.005 eV/Å. For the periodic calculations, the lattice parameters and atomic coordinates from literature (remdesivir Form II [24–26] tetrandrine orthorhombic [22] apilimod monoclinic [21]) were used as the initial structure. The electronic structure was calculated on a 3 × 2 × 3 Γ-centered grid for remdesivir, and Γ-point only for tetrandrine and apilimod. The optB86b-vdW dispersion-corrected functional [36] was applied. The vibrational eigenfrequencies and modes were computed by solving the force constants and dynamical matrix using Phonopy [37]. The OCLIMAX software [38] was used to convert the DFT-calculated phonon results to the simulated INS spectra. For the molecular calculations, the molecule was placed at the center of a cubic box. The size of the box is sufficiently large (20 Å) so that the interaction between the molecule and its image across the periodic boundaries is negligible, and the electronic structure was calculated on Γ-point only. The climbing image nudged elastic band (cNEB) method [39] was used to calculate the energy barrier for individual methyl group rotation directly. Seven images were introduced, with the starting and ending ones being the two equilibrium positions of

the methyl rotor separated by a relative rotation of 120°.

3. Results and discussion

3.1. Methyl group rotational tunneling and vibrations

Fig. 2 shows molecular and crystallographic unit cell structures for remdesivir, tetrandrine, and apilimod, featuring three, six, and one methyl groups per molecule, respectively. Using DFT calculations, we have identified and analyzed the methyl groups with the lowest rotational barrier in the crystal structures. For apilimod (Fig. 2 bottom), whose molecules have a single methyl group, both non-equivalent in the crystal structure methyl groups have been analyzed with two different positions in the crystal. From remdesivir to tetrandrine to apilimod, there is an evident decreasing trend in the lowest rotational barriers, both in the crystal structures and isolated molecules.

Fig. 3 shows the high energy-resolution spectra from tetrandrine and apilimod. Tetrandrine exhibits inelastic peaks positioned at about ± 18 μeV at the baseline temperature of 12 K that decrease in height, increase in width, and shift toward the elastic line as the temperature is increased, until at 35 K the peaks almost disappear in the growing quasielastic background. Apilimod similarly exhibits inelastic peaks, but they are positioned at about ± 8 μeV at the baseline temperature of 12 K. Because of the spectrometer's asymmetric resolution function, only the + 8 μeV feature can be resolved as a distinct peak. In contrast, the presence of its −8 μeV counterpart can only be inferred from the shoulder of the elastic peak that represents the spectrometer resolution as measured from a vanadium standard. Additionally, apilimod exhibits another inelastic peak positioned at about ± 80 μeV. As the temperature is increased, both the ± 8 μeV and ± 80 μeV peaks decrease in height, increase in width, and shift toward the elastic line, until at 35 K they almost disappear in the growing quasielastic background. Unlike apilimod and tetrandrine, remdesivir shows no inelastic or quasielastic signal at the measured temperature point of 20 K (the insets in Fig. 3) and, in the measured energy transfer range of ± 120 μeV, gives rise to the purely elastic scattering signal representing the resolution function, similar to the vanadium standard. The ± 18 μeV peaks in tetrandrine and the ± 8

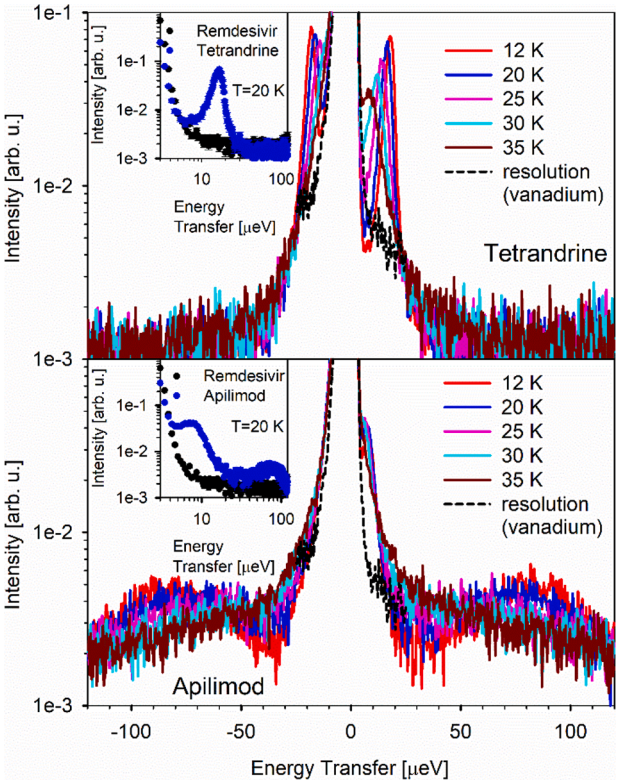

Fig. 3. Inelastic neutron scattering (INS) intensities, averaged for 0.2 $Å^{-1}$ < Q < 1.2 $Å^{-1}$, from tetrandrine (top panel) and apilimod (bottom panel) on the linear-logarithmic (main panels) and logarithmic-logarithmic scale (insets). Also shown are the scattering intensities from a vanadium standard (main panels) and remdesivir (insets); both vanadium and remdesivir represent the sample-dependent spectrometer resolution function, unlike tetrandrine and apilimod, which exhibit an inelastic or quasielastic signal. The data was collected at the BASIS spectrometer.

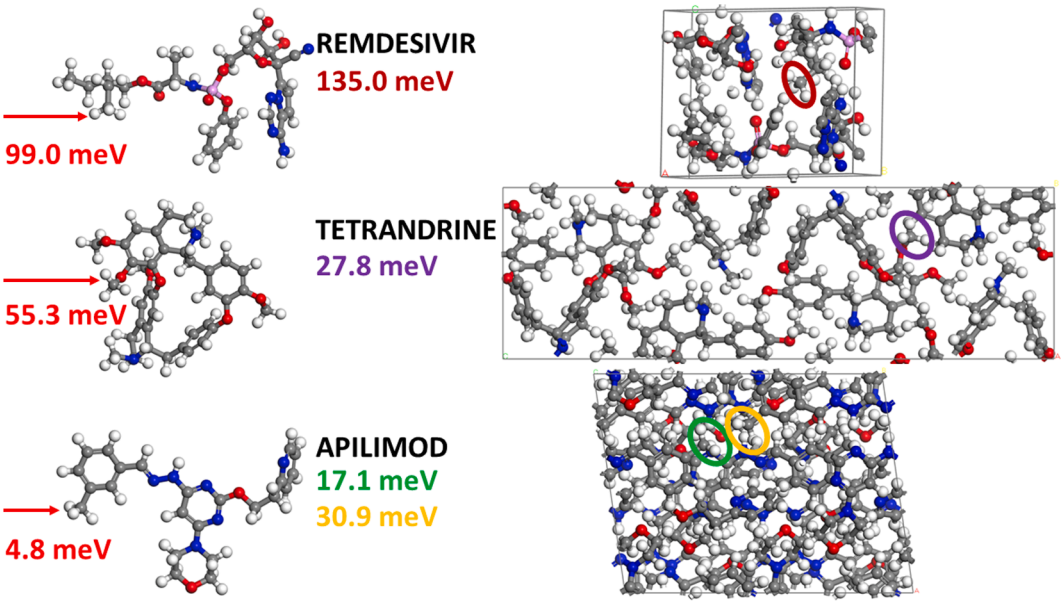

Fig. 2. Molecular and crystallographic unit cell structures of the antiviral drugs studied, remdesivir (top), tetrandrine (middle), and apilimod (bottom). For each drug, the methyl group with the lowest calculated rotational barrier in the crystal structure is marked by an ellipse, and the barrier height is indicated under the drug name using the same color. The corresponding methyl groups in the single molecules (considered before crystallization) are indicated by the red arrows, with the value of the associated barrier heights shown in red text. The apilimod molecules each have a single methyl group that assumes two non-equivalent positions in the crystal structure, as shown.

μeV/±80 μeV peaks in apilimod thus exhibit characteristic features of rotational quantum tunneling of methyl groups. It should be noted that a separate measurement at BASIS, with the same energy resolution and increased dynamic range (in the pulse-eliminating mode) has shown no additional tunneling peaks in tetrandrine within ± 200 μeV range, or even up to + 500 μeV in the one-sided asymmetric scattering spectrum.

Fig. 4 illustrates the relationship between the potential barrier height, tunneling energy, and librational energy. Also marked are the stochastic rotations, as measured by QENS at elevated temperatures. The expected methyl rotational barrier heights were estimated from the position of the tunneling peaks using the hindered rotor/methyl rotor tool in the Data Analysis and Visualization Environment (DAVE) software [40]. Specifically, for a rigid methyl rotor in a three-fold sinusoidal potential, the tunneling splitting and tunneling energy (as well as the excitation energy for libration) is a function of the barrier height. We can then adjust the barrier height until the solved tunneling energy matches the one measured in the experiment. Using this approach, we obtained barriers of 15 meV (from the 80 μeV tunneling peak) and 32 meV (from the 8 μeV tunneling peak) for apilimod and 25.3 meV (from the 18 μeV tunneling peak) for tetrandrine, in good agreement with the DFT-calculated potential barriers as presented in Fig. 2.

Furthermore, for these potential barriers, the expected first rotational excitations should be at 7.2 meV (for the methyl group that gives rise to the 80 μeV tunneling peak in apilimod), 12.0 meV (for the methyl group that gives rise to the 8 μeV tunneling peak in apilimod), and 10.3 meV (for the methyl group that gives rise to the 18 μeV tunneling peak in tetrandrine). The comparison of the INS data with the DFT calculations, as presented in Fig. 5, shows reasonably good agreement between the calculation and experiment, especially for apilimod. In reasonable agreement with the expectations based on the tunneling peaks position and the corresponding energy barriers, the DFT calculations predict the first rotational excitations at 6–7 meV (vs. expected 7.2 meV) and 13–18 meV (vs. expected 12.0 meV) in apilimod and 9.5–10.5 meV (vs. expected 10.3 meV) in tetrandrine. In contrast with the quantum tunneling peaks behavior, the inelastic peaks at higher energy transfers (the lowest one measured at about 3 meV, as presented in Fig. 5) exhibit characteristic features of vibrational excitations, such as an increase in intensity as the temperature is increased.

3.2. Methyl group stochastic rotational jumps

Above 35 K, the scattering signals collected at the BASIS spectrometer from tetrandrine and apilimod become quasielastic and can be fitted with a resolution-convolved superposition of a delta function and a Lorentz function, plus a linear background. The half-width at half-maximum (HWHM) of the fitted Lorentz function can be converted to the characteristic methyl rotational times, $\tau = \hbar/\mathrm{HWHM}$; they are presented in Fig. 6 along with the previously measured data for remdesivir

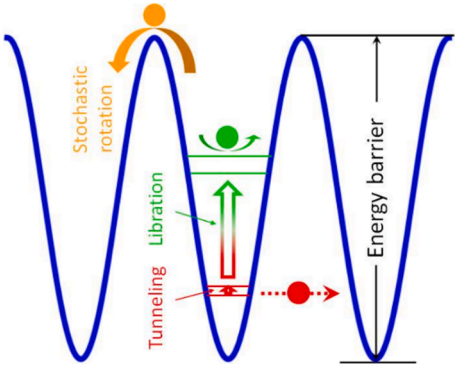

Fig. 4. A schematic illustration of the relationship between the potential barrier height, tunneling energy, and librational energy for methyls. Also shown are the stochastic rotational jumps at elevated temperatures.

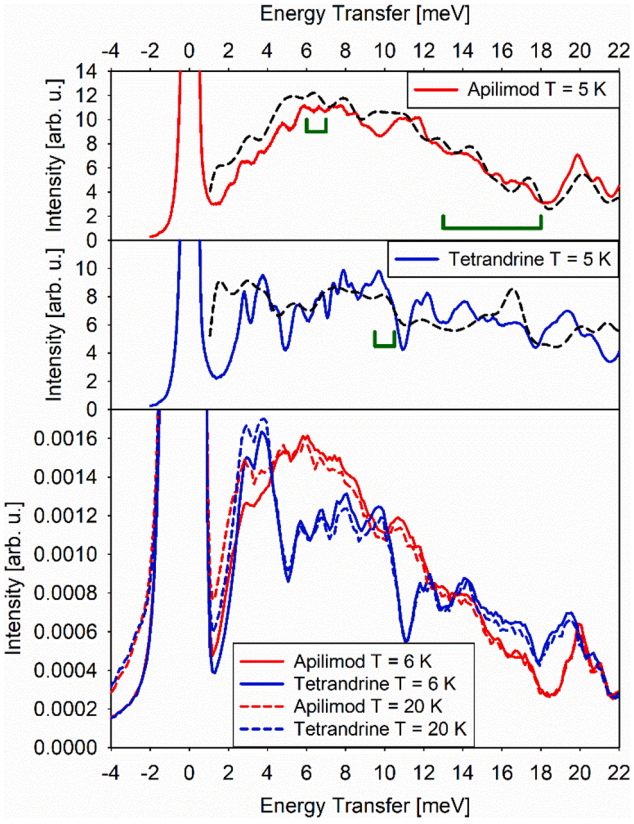

Fig. 5. Bottom panel: inelastic neutron scattering intensities measured from tetrandrine and apilimod with an incident neutron energy of 25 meV (averaged for 0.3 $Å^{-1}$ < Q < 3.1 $Å^{-1}$). The data were collected at the SEQUOIA spectrometer. Middle and top panels: inelastic neutron scattering intensities measured at the VISION spectrometer from tetrandrine and apilimod, respectively, and the corresponding DFT calculations of the vibrational spectra (black dashed lines). The square brackets show the positions of the torsional excitations associated with the methyl groups that give rise to the tunneling peaks at ± 18 μeV in tetrandrine and ± 8 μeV/±80 μeV in apilimod, as presented in Fig. 3.

[23]. The methyl rotational times in apilimod could be measured up to 80 K, above which the signal became too broad for the accessible energy transfer range of the spectrometer.

Unlike the apilimod molecule, which has a single methyl group, the tetrandrine molecule has six methyl groups. This explains an apparent non-monotonic temperature dependence of the methyl rotational time exhibited by tetrandrine in Fig. 6. Above 60 K, the quasielastic signal from the tetrandrine methyl groups with the lowest rotational barriers becomes too broad for the spectrometer. However, the other methyl group rotational signals gradually enter (and eventually exit) the spectrometer's accessible range of energy transfers, thereby giving rise to the apparent non-monotonic temperature dependence. It should be noted that even below 60 K the tetrandrine's methyl groups with the higher rotational barriers should also give rise to the quantum tunneling peaks, but at the energy transfers that would be within the resolution line of the neutron backscattering spectrometer used in the current measurements.

To identify the species that gives rise to the measured quasielastic signal, it is instructive to compute the elastic incoherent structure factor, EISF, (the ratio of the elastic to the total scattering intensities) and then compare it with an expression for 3-fold jumps [41] on a circle modified to allow for an additional parameter, c, describing the fraction of the "immobile" protons not participating in the rotational jumps, $\mathrm{EISF}(Q) = c+(1-c)(1 + 2j_0(Qd_{HH}))/3$, where j_0 is a spherical Bessel function of zeroth order, and d_{HH} is the distance between the protons on the circle. The expected value of d_{HH} for a methyl group is approximately 1.78 Å.

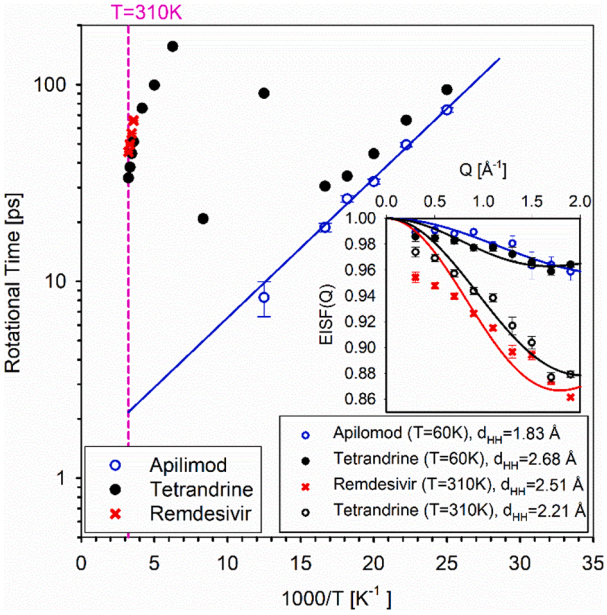

Fig. 6. Main panel: Arrhenius plot of the measured relaxation times (symbols) for the methyl group rotation in remdesivir (from Ref. 23), apilimod, and tetrandrine, τ as described in the main text. Inset: measured elastic incoherent structure factors (EISFs) and their best fits with the model for a methyl group rotation plus a background due to the protons not participating in the methyl group rotations. The data for the figure was collected at the BASIS spectrometer.

As shown in the Fig. 6 inset, only apilimod yields a fitted value close to that expected for a methyl group of (1.83 ± 0.36) Å, whereas for tetrandrine at 60 K, remdesivir at 310 K, and tetrandrine at 310 K, these values are (2.68 ± 0.12) Å, (2.51 ± 0.03) Å, and (2.21 ± 0.06) Å, respectively. This implies that only for apilimod can the measured quasielastic scattering signal be associated with a single methyl group rotation, whereas for tetrandrine or remdesivir, more than one methyl group must be contributing to the measured quasielastic signal. This conclusion is corroborated by the values of the "immobile" parameter, c, in the fit of EISF(Q). For remdisivir ($C_{27}H_{35}N_6O_8P$) at 310 K, c = (0.8359 ± 0.0016), suggesting measurable rotation of the two methyl groups out of three, for which the expected fraction of the "immobile" protons per molecule is 29/35 = 0.8286. For tetrandrine ($C_{38}H_{42}N_2O_6$) at 310 K, c = (0.8503 ± 0.0034), suggesting measurable rotation of the two methyl groups out of six, for which the expected fraction of the "immobile" protons per molecule is 36/42 = 0.8571.

Regarding the apilimod data as presented in Fig. 6, even though there are two non-equivalent methyl groups in the apilimod crystal structure, the one with a potential barrier of 32 meV (8 μeV tunneling peak) must be contributing to the resolution-limited elastic, as opposed to quasielastic signal, and the methyl group with a potential barrier of 15 meV (80 μeV tunneling peak) must be contributing to the measured quasielastic signal. This is corroborated by the value of the fit parameter (1-c) in the fit for EISF(Q), which is (0.0562 ± 0.0041), almost exactly one half of the value expected for the crystal structure where each methyl group (comprising 3 protons out of a total of 26 protons per molecule) contributes to the quasielastic signal (3/26 = 0.1154). Instead, only 50% of the methyl groups contribute to the measured quasielastic signal, namely those with the rotational barrier of 15 meV, whereas the contribution from the other 50% of the methyl groups, with the rotational barrier of 32 meV, lies within the elastic line. The conclusion that only one out of the two methyl groups in the apilimod crystal structure contributes to the quasielastic signal agrees with the fitted d_{HH} = (1.83 ± 0.36) Å being close to the expected value for a methyl group of 1.78 Å. As a consequence, the temperature dependence of the measured methyl rotational times in apilimod can be extrapolated to the physiological temperature of 310 K. The 310 K extrapolated methyl rotational time for apilimod (~2 ps) is a factor of 20 lower compared to remdesivir [23], possibly benefitting the biochemical and antiviral drug activity.

Our earlier studies [23,31] elaborated on the effect of hydration-induced disorder on reducing the methyl rotational barriers in water-soluble SARS-CoV-2 drug candidates. The importance of methyl group interactions with the solvent, e.g., in specific drug-kinase binding and ligand–protein binding in general, has been well recognized [42]. Simultaneously, the effect of hydration, while beneficial, may significantly complicate computational screening of drug candidates based on the methyl group potential barriers because the water molecules in the disordered aperiodic structure would have to be considered explicitly [42]. On the other hand, remdesivir and the supposedly more powerful antivirals, such as apilimod and tetrandrine, are insoluble in water. While their methyl groups cannot be lubricated in the same manner as the methyl groups in water-soluble drug molecules are lubricated by the hydration/solvation water, the computational screening of such water-insoluble drugs based on the methyl groups potential barriers becomes much more straightforward. The fact that the fitted values of the "immobile" parameter, c, are close to the values expected from the ratio of protons in the mobile methyl groups to the total number of protons per molecule strongly suggests that the measured quasielastic signals originate exclusively from the rotationally mobile methyl groups. In contrast, the other protons in the molecules contribute only to the elastic signal.

3.3. *Methyl group dynamics and bioactivity*

It should be noted that the potential barriers of 27.8 meV for tetrandrine and 17.1 and 30.9 meV for apilimod computed and experimentally validated in the present work are significantly lower than even the lowest potential barrier of 39.4 meV (3.8 kJ/mol) that we have previously measured for the hydrated water-soluble drug molecules [23,31]. Compared to the lowest calculated potential barrier for remdesivir of 135.0 meV, they are dramatically lower. One could argue that the potential barriers for methyl rotations in the isolated molecule, instead of the crystal structure, are of more direct significance to the biological activity of drugs *in vivo*. Indeed, in MD simulations, the methyl relaxation time was known to be hydration-dependent and scale with the diffusivity of the water model [43]. Such an argument is far from certain for the practically water-insoluble antivirals such as remdesivir, tetrandrine, and apilimod.

Nevertheless, even in such a case, isolated tetrandrine molecules exhibit dramatically lower barriers for methyl group rotations than isolated molecules of remdesivir, as presented in Fig. 2. Moreover, isolated molecules of apilimod exhibit even much lower (although not uniquely low for isolated molecules [44]) rotational barriers, as one can see in Fig. 2. This suggests that the low potential barriers for the most dynamically active methyl groups in apilimod and tetrandrine compared to remdesivir may not be explained solely based on the crystal structure packing density but may be attributed, at least in part, to the intramolecular factors.

In various systems, the high sensitivity of methyl rotational barriers to the local chemical environment could either impede or facilitate the rotation. A single molecule does not necessarily have the lowest barrier; depending on how its surroundings influence the molecular geometry, how nearby groups respond to or cooperate with the methyl rotation, and, ultimately, the local potential energy landscape, the barrier in a cluster or solid could be either higher or lower than in a single molecule [44,45].

Quantum tunneling had been demonstrated to contribute directly to the biochemical reaction rate at physiological temperatures (e.g., testosterone hydroxylation by human cytochrome P450 3A4 at 300 K [46] and many more examples in the literature [47]) and thus could be

important for the drug bioactivity. However, in the present case, we cannot assert the contribution of the quantum effects to the activity of apilimod and tetrandrine at physiological temperatures. At a minimum, the pronounced quantum effects observed herein for apilimod and tetrandrine manifest from the significantly reduced potential barriers. Thus, our results showcase the use of quantum methyl tunneling as a probe of the molecular energy landscape in drugs, similar to the earlier examples of studying the energy landscape in isostructural calcium channel blockers, nifedipine, nitrendipine, and nimodipine [48] as well as studies of stability in polymorphs of paracetamol [49]. On the other hand, the increase in the rate of the thermally activated stochastic jumps at physiological temperatures due to the reduced potential barriers could be genuinely significant for the drug bioactivity through the more efficient exploration of the energy landscape to sample the potentially thermodynamically favorable reaction states.

4. Conclusions

We conclude by noting that extensive numerical studies are significantly more time-efficient in screening for the low potential barriers in drug molecules than neutron scattering measurements for the same purpose. Screening studies aimed at establishing reliable drug efficacy trends must involve a large number of candidates [6]. Therefore, the apparent correlation between the previously reported higher efficacy of apilimod and tetrandrine and their lower potential barriers for the most dynamically active methyl groups compared to remdesivir, as demonstrated herein, can only be considered a suggestion, not proof. However, our study has successfully validated the prediction of the DFT-based calculations for the methyl group rotational barriers, demonstrating the high reliability of such calculations for molecular drugs. This should pave the way for the computational studies involving many antiviral compounds to fully understand the benefits of drug efficacy by lowering the potential barriers for methyl group rotations. There are many compounds with low potential barriers for methyl group rotations [50], and few of such compounds would exhibit the desired therapeutic effect. However, the goal of the computational screening studies would be to compare the barriers within a pre-selected class of molecules (e.g., antivirals), similar to the approach adopted in the experimental screening studies [6].

Declaration of Competing Interest

The authors declare that they have no known competing financial interests or personal relationships that could have appeared to influence the work reported in this paper.

Acknowledgments

The neutron scattering experiments at Oak Ridge National Laboratory's (ORNL's) Spallation Neutron Source (SNS) were supported by the Scientific User Facilities Division, Office of Science (Basic Energy Sciences), U.S. Department of Energy (DOE). The authors acknowledge the U.S. Department of Energy (DOE) Office of Science (Basic Energy Sciences) for research funding. M.R.R. acknowledges the National Energy Research Scientific Computing Center (NERSC), a U.S. Department of Energy (DOE) Office of Science User Facility, operated under Contract No. DE-AC02- 05CH11231, for access to supercomputing resources. Computing resources were also made available through the VirtuES and the ICEMAN projects, funded by the Laboratory Directed Research and Development Program of ORNL, managed by UT-Battelle, LLC for the U. S. Department of Energy under contract DE-AC05-00OR22725. The authors thank Dr. Mark D. Lumsden for valuable discussions. The authors are grateful to Rhonda Moody for dedication to obtaining sample materials.

References

[1] M.K. Lo, R. Jordan, A. Arvey, J. Sudhamsu, P. Shrivastava-Ranjan, A.L. Hotard, M. Flint, L.K. McMullan, D. Siegel, M.O. Clarke, R.L. Mackman, H.C. Hui, M. Perron, A.S. Ray, T. Cihlar, S.T. Nichol, C.F. Spiropoulou, GS-5734 and its parent nucleoside analog inhibit Filo-, Pneumo-, and Paramyxoviruses, Sci. Rep. 7 (1) (2017), https://doi.org/10.1038/srep43395.

[2] E.S. Amirian, J.K. Levy, Current knowledge about the antivirals remdesivir (GS-5734) and GS441524 as therapeutic options for coronaviruses, One Health 9 (2020) 100128, https://doi.org/10.1016/j.onehlt.2020.100128.

[3] R.E. Ferner, J.K. Aronson, Remdesivir in covid-19, BMJ. 369 (2020), m1610, https://doi.org/10.1136/bmj.m1610.

[4] A. Pizzorno, B. Padey, J. Dubois, T. Julien, A. Traversier, V. Dulière, P. Brun, B. Lina, M. Rosa-Calatrava, O. Terrier, In vitro evaluation of antiviral activity of single and combined repurposable drugs against SARS-CoV-2, Antiviral Res. 181 (2020) 104878, https://doi.org/10.1016/j.antiviral.2020.104878.

[5] F. Lamontagne, T. Agoritsas, H. Macdonald, Y.-S. Leo, J. Diaz, A. Agarwal, J. A. Appiah, Y. Arabi, L. Blumberg, C.S. Calfee, et al., A living WHO guideline on drugs for covid-19, BMJ. 370 (2020), m3379, https://doi.org/10.1136/bmj.m3379.

[6] L. Riva, S. Yuan, X. Yin, L. Martin-Sancho, N. Matsunaga, L. Pache, S. Burgstaller-Muehlbacher, P.D. De Jesus, P. Teriete, M.V. Hull, M.W. Chang, J.-W. Chan, J. Cao, V.-M. Poon, K.M. Herbert, K. Cheng, T.-T. Nguyen, A. Rubanov, Y. Pu, C. Nguyen, A. Choi, R. Rathnasinghe, M. Schotsaert, L. Miorin, M. Dejosez, T.P. Zwaka, K.-Y. Sit, L. Martinez-Sobrido, W.-C. Liu, K.M. White, M.E. Chapman, E.K. Lendy, R. J. Glynne, R. Albrecht, E. Ruppin, A.D. Mesecar, J.R. Johnson, C. Benner, R. Sun, P. G. Schultz, A.I. Su, A. García-Sastre, A.K. Chatterjee, K.-Y. Yuen, S.K. Chanda, Discovery of SARS-CoV-2 antiviral drugs through large-scale compound repurposing, Nature 586 (7827) (2020) 113–119, https://doi.org/10.1038/s41586-020-2577-1.

[7] C.Y. Kwan, F.I. Achike, Tetrandrine and related bis-benzylisoquinoline alkaloids from medicinal herbs: cardiovascular effects and mechanisms of action, Acta Pharmacol. Sin. 23 (2002) 1057–1068.

[8] Y. Sakurai, A.A. Kolokoltsov, C.-C. Chen, M.W. Tidwell, W.E. Bauta, N. Klugbauer, C. Grimm, C. Wahl-Schott, M. Biel, R.A. Davey, Two-pore channels control Ebola virus host cell entry and are drug targets for disease treatment, Science 347 (6225) (2015) 995–998, https://doi.org/10.1126/science:1258758.

[9] P.M. Heister, R.N. Poston, Pharmacological hypothesis: TPC2 antagonist tetrandrine as a potential therapeutic agent for COVID-19, Pharmacol. Res. Perspect. 8 (5) (2020), https://doi.org/10.1002/prp2.v8.510.1002/prp2.653.

[10] E.A. Nelson, J. Dyall, T. Hoenen, A.B. Barnes, H. Zhou, J.Y. Liang, J. Michelotti, W. H. Dewey, L.E. DeWald, R.S. Bennett, P.J. Morris, R. Guha, C. Klumpp-Thomas, C. McKnight, Y.-C. Chen, X. Xu, A. Wang, E. Hughes, S. Martin, C. Thomas, P. B. Jahrling, L.E. Hensley, G.G. Olinger, J.M. White, F. Kashanchi, The phosphatidylinositol-3-phosphate 5-kinase inhibitor apilimod blocks filoviral entry and infection, PLoS Negl. Trop. Dis. 11 (4) (2017) e0005540, https://doi.org/10.1371/journal.pntd.0005540.

[11] S. Qiu, A. Leung, Y. Bo, R.A. Kozak, S.P. Anand, C. Warkentin, F.D.R. Salambanga, J. Cui, G. Kobinger, D. Kobasa, M. Côté, Ebola virus requires phosphatidylinositol (3,5) bisphosphate production for efficient viral entry, Virology. 513 (2018) 17–28, https://doi.org/10.1016/j.virol.2017.09.028.

[12] Y.-L. Kang, Y.-Y. Chou, P.W. Rothlauf, Z. Liu, T.K. Soh, D. Cureton, J.B. Case, R. E. Chen, M.S. Diamond, S.P.J. Whelan, T. Kirchhausen, Inhibition of PIKfyve kinase prevents infection by Zaire ebolavirus and SARS-CoV-2, Proc. Natl. Acad. Sci. USA 117 (34) (2020) 20803–20813, https://doi.org/10.1073/pnas.2007837117.

[13] M.V. Baranov, F. Bianchi, G. van den Bogaart, The PIKfyve inhibitor apilimod: A double-edged sword against COVID-19, Cells 10 (2021) 30, https://doi.org/10.3390/cells10010030.

[14] M. Ospanov, F. Leon, J. Jenis, I. A. Khan, M. A. Ibrahim, Challenges and future directions of potential natural products leads against 2019-nCoV outbreak, Curr. Plant Biol. 24 (2020) 100180, doi: 10030 10.1016/j.cpb.2020.100180.

[15] H. Frauenfelder, G. Chen, J. Berendzen, P.W. Fenimore, H. Jansson, B. H. McMahon, I.R. Stroe, J. Swenson, R.D. Young, A unified model of protein dynamics, Proc. Nat. Acad. Sci. USA 106 (13) (2009) 5129–5134, https://doi.org/10.1073/pnas.0900336106.

[16] J.D. Nickels, J.E. Curtis, H. O'Neill, A.P. Sokolov, Role of methyl groups in dynamics and evolution of biomolecules, J. Biol. Phys. 38 (3) (2012) 497–505, https://doi.org/10.1007/s10867-012-9268-6.

[17] C.S. Leung, S.S.F. Leung, J. Tirado-Rives, W.L. Jorgensen, Methyl effects on protein-ligand binding, J. Med. Chem. 55 (9) (2012) 4489–4500, https://doi.org/10.1021/jm3003697.

[18] H. Schönherr, T. Cernak, Profound methyl effects in drug discovery and a call for new C-H methylation reactions, Angew. Chem. Int. Ed. 52 (47) (2013) 12256–12267, https://doi.org/10.1002/anie.201303207.

[19] K. Feng, R.E. Quevedo, J.T. Kohrt, M.S. Oderinde, U. Reilly, M.C. White, Late-stage oxidative C(sp(3))-H methylation, Nature 580 (7805) (2020) 621–627, https://doi.org/10.1038/s41586-020-2137-8.

[20] J. Colmenero, A.J. Moreno, A. Alegría, Neutron scattering investigations on methyl group dynamics in polymers, Prog. Polym. Sci 30 (12) (2005) 1147–1184, https://doi.org/10.1016/j.progpolymsci.2005.08.001.

[21] P.J. Morris, C. Moore, C.J. Thomas, IUCrData 2 (2017), x170693, https://doi.org/10.1107/S2414314617006939.

[22] Z. Zhou, H.H.Y. Tong, L. Li, F.L.Y. Shek, Y. Lv, Y. Zheng, Synthesis, crystal structures and phase transformation of the new solid-state forms of tetrandrine, RSC Advances 4 (107) (2014) 62586–62593, https://doi.org/10.1039/C4RA10457A.

[23] E. Mamontov, Y. Cheng, L.L. Daemen, A.I. Kolesnikov, A.J. Ramirez-Cuesta, M. R. Ryder, M.B. Stone, Hydration-induced disorder lowers the energy barriers for methyl rotation in drug molecules, J. Phys. Chem. Lett. 11 (23) (2020) 10256–10261, https://doi.org/10.1021/acs.jpclett.0c02642.
[24] D. Siegel, H.C. Hui, E. Doerffler, M.O. Clarke, K. Chun, L. Zhang, S. Neville, E. Carra, W. Lew, B. Ross, et al., CCDC 1525480: Experimental Crystal Structure Determination (2017), doi: 10.5517/ccdc.csd.cc1n6d19.
[25] D. Siegel, H.C. Hui, E. Doerffler, M.O. Clarke, K. Chun, L. Zhang, S. Neville, E. Carra, W. Lew, B. Ross, Q. Wang, L. Wolfe, R. Jordan, V. Soloveva, J. Knox, J. Perry, M. Perron, K.M. Stray, O. Barauskas, J.Y. Feng, Y. Xu, G. Lee, A. L. Rheingold, A.S. Ray, R. Bannister, R. Strickley, S. Swaminathan, W.A. Lee, S. Bavari, T. Cihlar, M.K. Lo, T.K. Warren, R.L. Mackman, Discovery and synthesis of a phosphoramidate prodrug of a Pyrrolo(2,1-f][triazin-4-amino] Adenine C-Nucleoside (GS-5734) for the treatment of Ebola and emerging viruses, J. Med. Chem. 60 (5) (2017) 1648–1661, https://doi.org/10.1021/acs.jmedchem.6b01594.
[26] K. Yu, S. Chen, C. Amgoth, G. Tang, H. Bai, X. Hu, Two polymorphs of remdesivir: crystal structure, solubility, and pharmacokinetic study, CrystEngComm 23 (16) (2021) 2923–2927, https://doi.org/10.1039/D1CE00175B.
[27] C. De Savi, D.L. Hughes, L. Kvaerno, Quest for a COVID-19 cure by repurposing small-molecule drugs: mechanism of action, clinical development, synthesis at scale, and outlook for supply, Org. Process Res. Dev. 24 (6) (2020) 940–976, https://doi.org/10.1021/acs.oprd.0c00233.
[28] E. Mamontov, K.W. Herwig, A time-of-flight backscattering spectrometer at the Spallation Neutron Source, BASIS, Rev. Sci. Instrum. 82 (8) (2011) 085109, https://doi.org/10.1063/1.3626214.
[29] G.E. Granroth, A.I. Kolesnikov, T.E. Sherline, J.P. Clancy, K.A. Ross, J.P.C. Ruff, B. D. Gaulin, S.E. Nagler, SEQUOIA: A newly operating chopper spectrometer at the SNS, J. Phys. Conf. Ser. 251 (2010) 012058, https://doi.org/10.1088/1742-6596/251/1/012058.
[30] A.J. Ramirez-Cuesta, Y. Cheng, Studying materials and processes with VISION, VirtuES and ICEMAN – Modeling INS data with DFT methods, Hamon 30 (2020) 154–159, https://doi.org/10.1063/1.3626214.
[31] E. Mamontov, Y. Cheng, L.L. Daemen, J.K. Keum, A.I. Kolesnikov, D. Pajerowski, A. Podlesnyak, A.J. Ramirez-Cuesta, M.R. Ryder, M.B. Stone, Effect of hydration on the molecular dynamics of hydroxychloroquine sulfate, ACS Omega 5 (33) (2020) 21231–21240, https://doi.org/10.1021/acsomega.0c0309110.1021/acsomega.0c03091.s001.
[32] G. Kresse, J. Furthmüller, Efficient iterative schemes for ab initio total-energy calculations using a plane-wave basis set, Phys. Rev. B 54 (16) (1996) 11169–11186, https://doi.org/10.1103/PhysRevB.54.11169.
[33] P.E. Blöchl, Projector augmented-wave method, Phys. Rev. B 50 (24) (1994) 17953–17979, https://doi.org/10.1103/PhysRevB.50.17953.
[34] G. Kresse, D. Joubert, From ultrasoft pseudopotentials to the projector augmented-wave method, Phys. Rev. B 59 (3) (1999) 1758–1775, https://doi.org/10.1103/PhysRevB.59.1758.
[35] J.P. Perdew, K. Burke, M. Ernzerhof, Generalized gradient approximation made simple, Phys. Rev. Lett. 77 (18) (1996) 3865–3868, https://doi.org/10.1103/PhysRevLett.77.3865.
[36] J. Klimeš, D.R. Bowler, A. Michaelides, Chemical accuracy for the van der Waals density functional, J. Phys.: Cond. Matt. 22 (2010) 022201, doi: 10.1088/0953-8984/22/2/022201.
[37] A. Togo, I. Tanaka, First principles phonon calculations in materials science, Scr. Mater. 108 (2015) 1–5, https://doi.org/10.1016/j.scriptamat.2015.07.021.
[38] Y.Q. Cheng, L.L. Daemen, A.I. Kolesnikov, A.J. Ramirez-Cuesta, Simulation of inelastic neutron scattering spectra using OCLIMAX, J. Chem. Theory Comput. 15 (3) (2019) 1974–1982, https://doi.org/10.1021/acs.jctc.8b01250.
[39] G. Henkelman, B.P. Uberuaga, H. Jónsson, A climbing image nudged elastic band method for finding saddle points and minimum energy paths, J. Chem. Phys. 113 (22) (2000) 9901–9904, https://doi.org/10.1063/1.1329672.
[40] R.T. Azuah, L.R. Kneller, Y. Qiu, P.L.W. Tregenna-Piggott, C.M. Brown, J.R. D. Copley, R.M. Dimeo, DAVE: A comprehensive software suite for the reduction, visualization, and analysis of low energy neutron spectroscopic data, J. Res. Natl. Inst. Stan. Technol. 114 (6) (2009) 341, https://doi.org/10.6028/jres10.6028/jres.114.025.
[41] M. Bée, Quasielastic Neutron Scattering, Hilger, Bristol, 1988.
[42] B. Wienen-Schmidt, D. Schmidt, H.-D. Gerber, A. Heine, H. Gohlke, G. Klebe, Surprising non-additivity of methyl groups in drug-kinase interaction, ACS Chem. Biol. 14 (12) (2019) 2585–2594, https://doi.org/10.1021/acschembio.9b00476.
[43] F. Hoffmann, M. Xue, L.V. Schäfer, F.A.A. Mulder, Narrowing the gap between experimental and computational determination of methyl group dynamics in proteins, Phys. Chem. Chem. Phys. 20 (38) (2018) 24577–24590, https://doi.org/10.1039/C8CP03915A.
[44] J. Baudry, van der waals interactions and decrease of the rotational barrier of methyl-sized rotators: A theoretical study, J. Am. Chem. Soc. 128 (2006) 11088–11093, https://doi.org/10.1021/ja060731k.
[45] S. Khazaei, D. Sebastiani, Methyl rotor quantum states and the effect of chemical environment in organic crystals: gamma-picoline and toluene, J. Chem. Phys. 145 (2016), 234506, https://doi.org/10.1063/1.4971380.
[46] Y. Zhang, H. Lin, Quantum tunneling in testosterone 6β-hydroxylation by Cytochrome P450: Reaction dynamics calculations employing multiconfiguration molecular-mechanical potential energy surfaces, J. Phys. Chem. A 113 (43) (2009) 11501–11508, https://doi.org/10.1021/jp901850c.
[47] J.P. Klinman, A new model for the origin of kinetic hydrogen isotope effects, J. Phys. Org. Chem 23 (2010) 606–612, https://doi.org/10.1002/poc.1661.
[48] K. Druzbicki, A. Pajzderska, A. Kiwilsza, J. Jenczyk, D. Chudoba, M. Jarek, J. Mielcarek, J. Wasicki, In search of the mutual relationship between the structure, solid-state spectroscopy and molecular dynamics in selected calcium channel blockers, Eur. J. Pharmaceut. Sci. 85 (2016) 68–83, https://doi.org/10.1016/j.ejps.2016.01.024.
[49] N. Tsapatsaris, S. Landsgesell, M.M. Koza, B. Frick, E.V. Boldyreva, H.N. Bordallo, Polymorphic drugs examined with neutron spectroscopy: Is making more stable forms really that simple? Chem. Phys. 427 (2013) 124–128, https://doi.org/10.1016/j.chemphys.2013.04.016.
[50] M. Prager, A. Heidemann, Rotational tunneling and neutron spectroscopy: A compilation, Chem. Rev. 97 (1997) 2933–2966, https://doi.org/10.1021/cr9500848.